Synthesis of New Sn-Incorporated Layered Double Hydroxides and Their Thermal Evolution to Mixed Oxides

S. Velu, K. Suzuki,* M. Okazaki, T. Osaki, S. Tomura, and F. Ohashi

Ceramics Technology Department, National Industrial Research Institute of Nagoya, 1-1 Hirate-cho, Kita-ku, Nagoya 462-8510, Japan

Received February 1, 1999. Revised Manuscript Received May 20, 1999

A new series of $Mg^{II}Al^{III}Sn^{IV}$ hydrotalcite (HT)-like layered double hydroxides (LDHs) with Mg:Al:Sn = 3:1:0 to 3:0:1 were synthesized for the first time by a simple coprecipitation method at room temperature. The physicochemical properties of both as-synthesized and their thermally decomposed products were investigated in detail by various analytical and spectroscopic methods such as powder X-ray diffraction (PXRD), chemical analysis, scanning electron microscopy (SEM), FT-IR spectroscopy, ^{119}Sn and ^{27}Al MAS NMR, simultaneous TG/DTA, and N_2 adsorption−desorption experiments. A single phase corresponding to LDH could be obtained in the composition range Mg:Al:Sn = 3:1:0 to 3:0.7:0.3. Above this composition, in addition to LDH, the $MgSn(OH)_6$ phase also was formed. The ^{119}Sn NMR showed a broad signal in the range −525 to −660 ppm for Sn atoms existing in a distorted octahedral environment. Thermal calcination of MgAlSn-LDHs at 450 or 700 °C resulted in the formation of MgO-like solid solution, in which both Al^{3+} and Sn^{4+} were dissolved. The surface area and pore volume had decreased with increasing Sn content for both as-synthesized and calcined samples. Calcination at 1100 °C yielded a mixture of well-crystallized phases corresponding to MgO, $MgAl_2O_4$, and Mg_2SnO_4 "inverse spinel".

Introduction

Layered double hydroxides (LDHs) or synthetic anionic clays having hydrotalcite (HT)-like structure are receiving increasing interest in recent years owing to their potential applications in various technologies as ion exchangers, adsorbents, ionic conductors, catalysts, and catalyst supports.[1−5] The structure of LDHs was first elucidated by Allmann[6] for the MgFe-LDH (pyroaurite and sjögrenite) and by Brown et al.[7] for the MgAl-LDH (hydrotalcite and manasseite). These compounds are viewed as buildup from positively charged brucite $[Mg(OH)_2]$-like octahedral layers in which a part of M(II) cations are isomorphously substituted by a M(III) cation. The excess positive charge of the octahedral layers resulting from this substitution is compensated by interstitial layers built up of CO_3^{2-} anions and crystal water. These compounds are described by the general formula $[M(II)_{1-x}M(III)_x(OH)_2]^{x+}[(A^{n-})_{x/n}y\cdot H_2O]^{x-}$, where M(II) is a divalent cation (e.g., Mg, Cu, Ni, Co, Zn, etc.), M(III) is a trivalent cation (e.g., Al, Fe, Cr, Ga, Ru, Rh), and A^{n-} is the interlayer charge-compensating anion such as CO_3^{2-}, NO_3^-, Cl^-, etc. A large number of LDHs with a wide variety of M(II)−M(III) cation pairs as well as M(I)−M(III) cation pair (e.g., Li−Al) with different anions in the interlayer and their physicochemical properties have been reported.[8−10] However, LDHs containing a M(IV) cation in the brucite-like layer and their detailed physicochemical properties are scarce in the literature. CoTi-LDH was the only compound, synthesized by Taylor[11] using an induced hydrolysis method. However, the detailed physicochemical properties of the material are not described. In our recent reports we have shown that tetravalent cations such as Zr^{4+} could be effectively incorporated in the brucite-like layer in a wide composition range, and the resulting LDHs are active as a catalyst for liquid-phase hydroxylation of phenol.[12,13]

The aim of the present investigation is to synthesize a new series of Sn-incorporated MgAl-LDHs and to study the physicochemical properties of both as-synthesized and their thermally derived products. The general interest in the synthesis of these Sn-incorporated LDHs stem from the fact that, similar to zeolites containing Sn (Sn-silicalites, Sn-FSM-16),[14,15] these compounds

(1) Vaccari, A. *Catal. Today* **1998**, *41*, 53.
(2) Yun, S. K.; Pinaavaia, T. J. *Chem. Mater.* **1995**, *7*, 348.
(3) Moreyron, J. E.; de Roy, A.; Forano, C.; Besse, J. P. *Appl. Clay Sci.* **1995**, *10*, 163.
(4) Auer, S. M.; Wandeler, R.; Gobel, U.; Baiker, A. *J. Catal.* **1997**, *169*, 1.
(5) Basile, F.; Basini, L.; Amore, M. D.; Fornasari, G.; Guarinoni, A.; Matteuzzi, D.; Piero, G. D.; Trifiro, F.; Vaccari, A. *J. Catal.* **1998**, *173*, 247.
(6) Allmann, R. *Acta Crystallogr.* **1968**, *B24*, 972.
(7) Brown, G.; Gastuche, M. C. *Clay Miner.* **1967**, *7*, 193.
(8) Bellotto, M.; Rebours, B.; Clause, O.; Lynch, J.; Bazin, D.; Elkaim, E. *J. Phys. Chem.* **1996**, *100*, 8527.
(9) Basil, F.; Basini, L.; Fornasari, G.; Gazzano, M.; Trifiro, F.; Vaccari, A. *Chem. Commun.* **1996**, 2435.
(10) Fernandez, J. M.; Ulibarri, M. A.; Labojos, F. M.; Rives, V. *J. Mater. Chem.* **1998**, *8*, 2507.
(11) Taylor, M. *Clay Miner.* **1984**, *19*, 591.
(12) Velu, S.; Veda Ramasamy; Ramani, A.; Chanda, B. M.; Sivasanker, S. *Chem. Commun.* **1997**, 2107.
(13) Velu, S.; Sabde, D. P.; Shah, N.; Sivasanker, S. *Chem. Mater.* **1998**, *10*, 3451.
(14) Mal, N. K.; Ramasamy, A. V. *Chem. Commun.* **1997**, 425.

10.1021/cm990067p CCC: $18.00
Published on Web 07/14/1999

Table 1. Chemical Composition, Lattice Parameters, and Structural Properties of MgAlSn-LDHs[f]

sample	Mg:Al:Sn atomic ratio[a]	Mg/(Al + Sn)	PXRD phase obtained	lattice parameters[b] (Å) *a*	lattice parameters[b] (Å) *c*	fwhm[c] (2θ)	*t*[d] (Å)	chemical formula[e]
Sn 0-LDH	3:0.90:0.00	3.33	LDH	3.053	23.543	0.893	176	$Mg_6Al_{1.80}Sn_{0.00}(OH)_{16}(CO_3)_{0.70}3.7H_2O$
Sn 1-LDH	3:0.80:0.09	3.37	LDH	3.056	23.405	1.071	160	$Mg_6Al_{1.60}Sn_{0.18}(OH)_{16}(CO_3)_{0.76}3.7H_2O$
Sn 2-LDH	3:0.71:0.19	3.33	LDH	3.064	23.354	1.250	129	$Mg_6Al_{1.42}Sn_{0.38}(OH)_{16}(CO_3)_{0.89}3.9H_2O$
Sn 3-LDH	3:0.70:0.29	3.03	LDH	3.067	23.349	1.643	96	$Mg_6Al_{1.40}Sn_{0.58}(OH)_{16}(CO_3)_{1.26}5.9H_2O$
Sn 4-LDH	3:0.54:0.37	3.30	LDH + MHS	3.082	23.444	1.429		
Sn 5-LDH	3:0.44:0.45	3.37	LDH + MHS	3.091	23.441	1.429		
Sn 7-LDH	ND		LDH + MHS		23.452			
Sn 10-LDH	3:0.00:0.96	3.13	LDH + MHS		23.452			
Al 7-LDH	3:0.70:0.00	4.29	LDH	3.068	23.562	1.22	129	$Mg_6Al_{1.40}(OH)_{16}(CO_3)_{0.2}2.9H_2O$

[a] Determined by X-ray fluorescence (XRF) spectroscopy. [b] Lattice parameters *a* and *c* of LDH phase calculated from *d*(110) and *d*(003) planes, respectively. [c] Full width at half-maximum (fwhm) of (003) plane. [d] Average crystallite size calculated from (003) and (006) planes using the Debye−Scherrer equation. [e] Chemical formula of LDH phase calculated based on XRF and TG results. [f] LDH = layered double hydroxide phase, MHS = magnesium hydroxostannate [$MgSn(OH)_6$] phase, ND = not determined.

would serve as a catalyst for several oxidation reactions in the synthesis of fine chemicals. Furthermore, several Sn-containing mixed oxide systems have been widely employed as an efficient catalyst for a variety of organic transformations.[16,17]

Experimental Section

Synthesis of Sn-Incorporated LDHs. Sn-containing LDHs with various Mg:Al:Sn atomic ratio were synthesized by a coprecipitation method at room temperature by reacting aqueous solutions containing a mixture of $Mg(NO_3)_2$, $Al(NO_3)_3$, and $SnCl_4$ salts (depending upon the Mg:Al:Sn atomic ratio) and a mixture of NaOH (≈2 M solution) and Na_2CO_3 (≈0.3 M solution) at a constant pH (≈9).[12] The Mg/(Al + Sn) atomic ratio in the starting solution was kept as 3 while varying the Al:Sn ratio from 1:0 to 0:1. The resulting precipitate was aged at 65 °C for 30 min under stirring in a magnetic stirrer, then filtered, washed with deionized water several times until the pH of the filtrate was 7, and then dried in an air oven at 70 °C overnight.

Materials Characterization. The chemical compositions of the samples were determined by X-ray fluorescence (XRF) spectroscopy (Shimadzu Co. Lab center, XRF-1700 sequential X-ray fluorescence spectrometer). The powder X-ray diffraction (PXRD) of the samples was carried out using a Rigaku instrument (model RAD-1 VC) equipped with a Ni-filtered Cu Kα radiation (λ = 1.5418 Å). The data were collected in the 2θ range 5−70° with a scan rate of 1° 2θ/min for calculation of lattice parameters, while a speed of 2°/min was used for obtaining the PXRD patterns. The observed interplanar *d* spacing was corrected using elemental Si as an internal standard [*d*(111) = 3.1355 Å; JCPDS file no. 27-1402]. SEM micrographs were obtained with a Hitachi S-2300 scanning electron microscope. The samples were initially dispersed ultrasonically in ethanol, and a few drops of the suspension were applied onto the Al sample holder and coated with platinum before examination. FT-IR spectra were recorded using a Jasco FT-IR 620 instrument in the range 400−4000 cm^{-1} with a resolution of 4 cm^{-1}. ^{119}Sn and ^{27}Al solid-state NMR observations were made with a Bruker MSL-200 spectrometer. The sample was packed in a 7.0 ϕ spinner and spun at about 3.0 kHz at the magic angle. Free induction decay was accumulated after the excitation pulse with or without high-power proton decoupling. Duration of the excitation of radio-frequency pulse was adjusted well below the 90° pulse. The cross-polarization technique was not employed. A recycle delay of 30 and 4 s was employed for Sn and Al nuclei, respectively. The total data points were 8K words. Pure SnO_2 was used as a secondary reference to correct the chemical shift values in ^{119}Sn NMR spectra, while the chemical shift of a 1 M aqueous solution of $Al(NO_3)_3$ was taken as a reference in ^{27}Al MAS NMR. Simultaneous TG/DTA experiments were performed on a SSC/5200, SII Seiko instruments in the temperature range 50−700 °C with a scan rate of 10 °C/min in a N_2 atmosphere. N_2 adsorption−desorption experiments were carried out at 77 K using a Belsorp 28 SA (Japan) automatic gas adsorption apparatus. The surface area of the samples was calculated using the BET equation, while the Dollimore−Heal method was employed for the calculation of pore size.

Results and Discussion

As-Synthesized Materials. Table 1 summarizes the chemical composition, lattice parameter, and structural properties of a series of MgAlSn-LDHs with Mg:Al:Sn = 3:1:0 to 3:0:1 (Sn 0-LDH to Sn 10-LDH), while their PXRD patterns are presented in Figure 1. The Mg:Al:Sn atomic ratio determined by the XRF spectroscopy (Table 1) is coincident, within the experimental errors, with those of the starting mixed aqueous solutions. The experimental Mg/(Al + Sn) ratio is 3.2 ± 0.2 for all the samples, which is very close to 3 (except for Al 7-LDH), the expected theoretical ratio, taken in the starting mixed aqueous solution. The sample Al 7-LDH has been synthesized by keeping the same Mg:Al atomic ratio as that of Sn 3-LDH, but without mixing $SnCl_4$ salt. The observed results indicate that, under the preparation conditions employed in the present study, all the metal cations are completely coprecipitated.

The PXRD patterns (Figure 1) of these Sn-containing samples exhibit diffraction patterns characteristic of LDHs phase (JCPDS file no. 22-700) in the composition range Mg:Al:Sn = 3:1:0 to 3:0.7:0.3 (Sn 0-LDH to Sn 3-LDH). Above this composition, in addition to the LDHs phase, a cubic phase corresponding to magnesium hydroxostannate (MHS; $MgSn(OH)_6$, JCPDS file no. 9-27) is noticed. The incorporation of Sn^{4+} in the layers of LDH can be assessed from changes in the lattice parameters *a* and *c*, since a part of Al^{3+} (ionic radius 0.53 Å) is isomorphously substituted by Sn^{4+} (ionic radius 0.69 Å).[18] The parameter *a* of LDHs correspond to the cation−cation distance within the brucite-like layer and can be calculated as, $a = 2d(110)$.[19] On the

(15) Kitayama, Y.; Asano, H.; Kodama, T.; Abe, J.; Tsuchiya, Y. *J. Porous Mater.* **1998**, *5*, 139.
(16) Gomez, R.; Sanchez, J.; Silva, R.; Lopez, T. *React. Kinet. Catal. Lett.* **1996**, *59*, 247.
(17) Stork, S.; Maier, W. F.; Salrado, I. M. M.; Ferreria, J. M. F.; Guhl, D.; Souverijns, W.; Martens, J. A. *J. Catal.* **1997**, *172*, 414.
(18) Shannon, R. D. *Acta Crystallogr., Sect. A* **1976**, *32*, 751.
(19) del Arco, M.; Trujillano, R.; Rives, V. *J. Mater. Chem.* **1998**, *8*, 761.

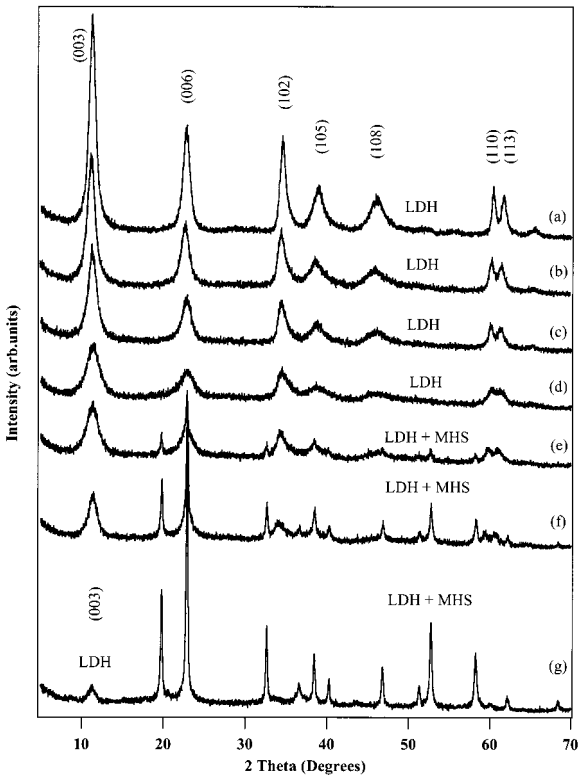

Figure 1. PXRD patterns of (a) Sn 0-LDH, (b) Sn 1-LDH, (c) Sn 2-LDH, (d) Sn 3-LDH, (e) Sn 5-LDH, (f) Sn 7-LDH, and (g) Sn 10-LDH; (LDH) = layered double hydroxide, (MHS) = $MgSn(OH)_6$.

other hand, the *c* parameter depends on several factors such as the anion size, extent of hydration, amount of interlayer anion, etc. However, for LDHs with the same M(II)−M(III)/M(IV) homologue series prepared under similar experimental conditions, the *c* parameter can be related to the thickness of the brucite-like layer and the interlayer distance and can be obtained from $c = 3d(003)$.[19] It can be seen from Table 1 that the *a* parameter increases with increasing Sn content, whereas the *c* parameter decreases with increase in Sn content only up to Sn 3-LDH and then remains almost unchanged. The increase in *a* parameter clearly indicates the incorporation of Sn^{4+} in the brucite-like layer. However, a large increase in *a* parameter even beyond Sn 3-LDH composition, where a MHS phase also is formed in addition to the LDH phase, is unexpected. This may be due to the imprecise determination of the position of the *d*(110) peak because of the low crystallinity of the sample. The decrease in *c* parameter from Sn 0-LDH to Sn 3-LDH can be attributed to the increase of the attractive force between the brucite-like layer and the interlayer. This is because of an increase in charge density of the brucite-like layer since a trivalent cation Al^{3+} is isomorphously substituted by a tetravalent cation Sn^{4+}. Further addition of Sn^{4+} leads to the crystallization of mainly the MHS phase; hence, the *c* value of LDH remains almost unchanged.

It can also be noticed from Figure 1 that the intensity or sharpness of all the peaks corresponding to the LDH phase decreases with increasing Sn content in the sample. Furthermore, the Sn-substituted samples exhibit broader diffraction lines, probably indicating a smaller scattering domain size. As a measure of crystallinity of the LDH phase in the *c*-axis direction, the full width at half-maximum (fwhm) value of the (003) plane is included in Table 1. The increase in the fwhm value of the (003) line from Sn 0-LDH to Sn 3-LDH demonstrates that the crystallinity of the LDH phase decreases upon incorporation of Sn in the LDH framework. The decrease in fwhm values at higher Sn content could be due to the coformation of the MHS phase in addition to the LDH phase. The average crystallite size of the compounds have also been calculated from the (003) and (006) planes employing the Debye−Scherrer equation,[20] $t = 0.9\lambda/\beta \cos\theta$, where *t* is the crystallite size, λ is the wavelength of the radiation used, β is the full width at half-maximum (fwhm) in radians, and θ is the Bragg diffraction angle, and the values are gathered in Table 1. It can be seen that the crystallite size decreases with increase in Sn content in the sample. The decrease in crystallinity and the crystallite size with increasing Sn content reveals the isomorphous substitution of a part of Al^{3+} (ionic radius 0.53 Å) by Sn^{4+} (ionic radius 0.69 Å). Such an isomorphous substitution would introduce distortion in the brucite-like layer, thereby reducing the compound crystallinity. However, it has been known that in the case of MgAl-LDH systems the crystallinity decreased when the Mg/Al atomic ratio increased (decrease in Al content).[21] For the purpose of investigating whether the decrease in crystallinity of these Sn-incorporated LDHs is due to the incorporation of Sn^{4+} or increase in the Mg/Al atomic ratio in the brucite-like layer, we have also synthesized another sample with the same Mg/Al atomic ratio (Al 7-LDH) as that of Sn 3-LDH, but without mixing Sn salt. The structural properties of Al 7-LDH (Mg:Al:Sn = 3:0.7:0) are included in Table 1 itself for a better comparison. It should be stressed that if Sn^{4+} had not been incorporated in the brucite-like layer, the same crystallinity would be anticipated for both Sn 3-LDH and Al 7-LDH. In contrast, the fwhm value of Al 7-LDH (1.22° 2θ) is considerably smaller than that of Sn 3-LDH (1.643° 2θ). Furthermore, the observed that the integral peak intensity of Al 7-LDH is nearly twice that of Sn 3-LDH (PXRD of Al 7-LDH is not shown). These results demonstrate that the decrease in crystallinity is due to the incorporation of Sn^{4+} in the brucite-like layer. Additionally, a large decrease in the *c* value (0.213 Å) as well as the crystallite size (33 Å) upon Sn incorporation (compare the *c* and the *t* values of Sn 3-LDH and Al 7-LDH in Table 1) substantiates the above conclusion. One can also doubt that, since the (200) peak around $2\theta = 23°$ (the most intense peak) of MHS phase coincides with that of (006) of LDH, a small amount of MHS phase could be present in Sn 3-LDH. Interestingly, the observed relative integral intensity ratio between (003) and (006) lines in this sample is 2:1, which is a characteristic of LDHs with HT-like structure. On the basis of these facts, it can be concluded that pure HT-like LDH phase could be obtained up to Sn 3-LDH (Mg:Al:Sn = 3:0.7:0.3). A further increase in Sn^{4+} content leads to the crystallization of the MHS phase in addition to the LDH phase. Another interesting observation noticed from the PXRD of these materials is that the sample Sn 10-LDH, without Al, also exhibits the *d*(003)

(20) Cullity, B. D. *Elements of X-ray diffraction*; Addition-Wesley: Reading, MA, 1959.
(21) Velu, S.; Swamy, C. S. *Appl. Catal. A: General* **1994**, *119*, 241.

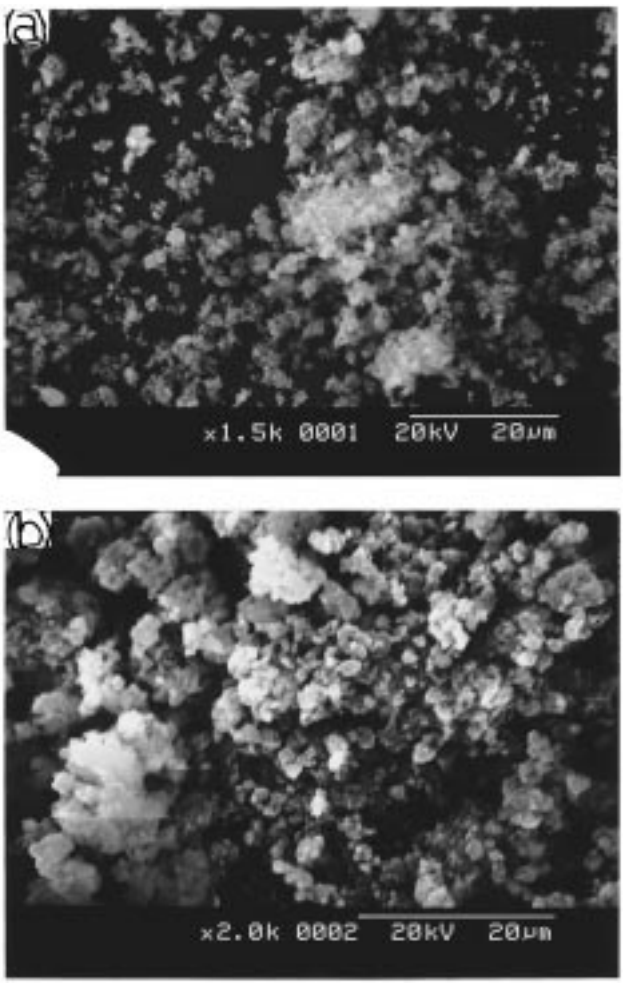

Figure 2. SEM micrographs of (a) Sn 3-LDH and (b) Al 7-LDH.

peak of LDH around 11° 2θ (see Figure 1g). This is in contrast to our earlier results on the similar Zr^{4+}-incorporated LDHs, wherein an X-ray amorphous phase was noticed if Al^{3+} was not present in the sample.[13]

Scanning electron microscopy (SEM) micrographs of some of these compounds were taken to get an insight into the topographic features. Figure 2 shows the SEM images of Sn 3-LDH and Al 7-LDH. Both show small spherical to hexagonal plateletlike particles, which are agglomerated. Although it was not possible to determine the particle size of these compounds from SEM, it can be viewed from the figure that Al 7-LDH is composed of relatively bigger particles than the Sn 3-LDH, which is in line with the PXRD results.

FT-IR spectroscopy is generally employed to identify the nature of interlayer anions present in these materials. It can also provide information regarding the purity of the compound. The FT-IR spectra of some of the Sn-containing LDHs are shown in Figure 3. The Sn 0-LDH, without Sn, shows characteristic bands for MgAl-LDH intercalated with CO_3^{2-} as the counteranion. A broad and intense band around 3500 cm^{-1} is observed, which is attributed to the stretching vibration of the hydroxyl (OH) groups in the layer and of water molecules (ν_{OHstr}). The corresponding deformation mode is recorded around 1650 cm^{-1}. IR absorptions due to the ν_2 (out-of-plane deformation), ν_3 (asymmetric stretching), and ν_4 (in-plane bending) of CO_3^{2-} ion existing in the interlayer

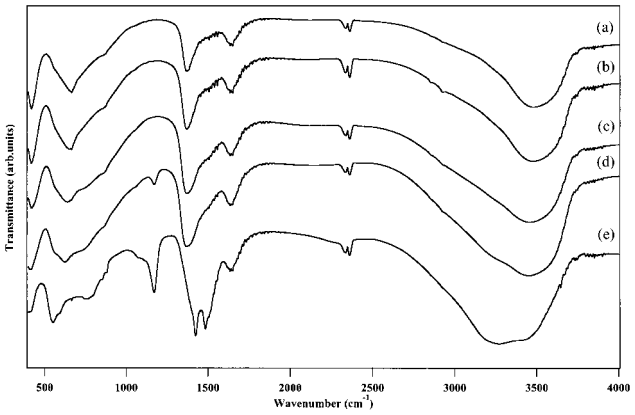

Figure 3. FT-IR spectra of (a) Sn 0-LDH, (b) Sn 1-LDH, (c) Sn 3-LDH, (d) Sn 5-LDH, and (e) Sn 10-LDH.

are observed around 870, 1370, and 660 cm^{-1}, respectively. The other bands less than 1000 cm^{-1} are generally ascribed to the M−O− skeletal vibrations.[13,19] The Sn-substituted LDHs (Sn 1-LDH to Sn 3-LDH) also exhibit similar IR features for Sn-incorporated MgAl-LDHs. However, differences are noticed in the relative intensity and sharpness of the bands upon Sn incorporation. For example, (i) small shifts in ν_{OHstr} toward lower wavenumber from around 3459 cm^{-1} for Sn 0-LDH to 3420 cm^{-1} for Sn 3-LDH. This is presumably because of the lowering of electron density around OH groups, which are coordinated to Sn^{4+} cations. (ii) The fwhm of the ν_{OHstr} increases from 368 cm^{-1} for Sn 0-LDH to 560 cm^{-1} for Sn 3-LDH and can be attributed to an increase in the cation distribution[22] due to the incorporation of Sn in the brucite-like layer. (iii) An increase in sharpness of the ν_3 of CO_3^{2-} band, as its content increases with increase in Sn content in the sample (see the molecular formula in Table 1). Differences in FT-IR absorptions are observed for samples Sn 5-LDH to Sn 10-LDH, for which the PXRD showed the presence of the MHS phase, in addition to the LDH phase. It can be seen that an additional intense and broad band at 3276 cm^{-1} together with a sharp band at 1172 cm^{-1} is recorded in Sn 10-LDH. These two bands are attributed to the ν_{OHstr} and ν_{OHbend} of OH groups of $MgSn(OH)_6$. This conclusion has been derived from the fact that the M−OH bending in the $[Sn(OH)_6]^{2-}$ ion appears[23] around 1150 cm^{-1}. The ν_3 and ν_4 of interlayer CO_3^{2-} ion are absent in this compound because of the absence of the layer structure. Instead, it exhibits a doublet at 1475 and 1425 cm^{-1}, which is very close to that of free CO_3^{2-} species (1415 cm^{-1}). Hence, the doublet would correspond to the CO_3^{2-} ion adsorbed on the $MgSn(OH)_6$ basic surface.

To investigate the local chemical environment of Sn and Al in the brucite-like layer, both ^{119}Sn and ^{27}Al MAS NMR studies have been undertaken. Since the ^{119}Sn is a heavier spin $^1/_2$ nuclei, its large chemical shift anisotropy leads to low sensitivity as the NMR signals are dispersed into a large number of spinning sidebands. Hence, the ^{119}Sn MAS NMR was recorded only for a few

(22) Hernandez-Moreno, M. J.; Ulibarri, M. A.; Rendon, J. L.; Serna, C. *J. Phys. Chem. Mineral.* **1985**, *12*, 34.
(23) Nakamoto, K. *Infrared and Raman Spectra of Inorganic and Coordination Compounds*, 3rd ed.; John Wiley and Sons: New York, 1978.

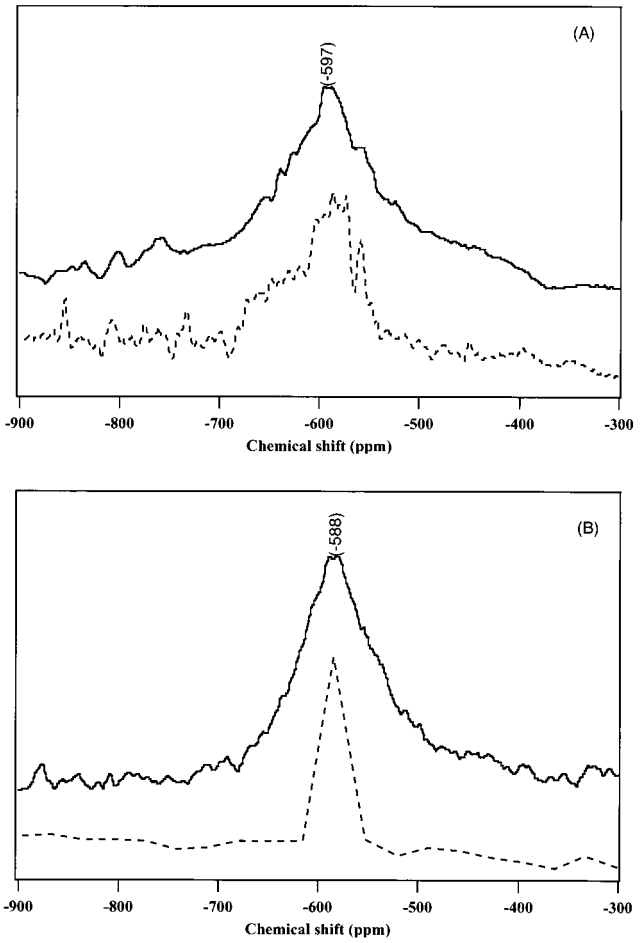

Figure 4. ^{119}Sn MAS NMR spectra of (A) Sn 3-LDH and (B) Sn 10-LDH. Solid line, without proton decoupling; dotted line, with proton decoupling.

selected samples. Figure 4 shows the ^{119}Sn NMR spectra of Sn 3-LDH and Sn 10-LDH observed with/without proton decoupling. In both samples, the spectra without proton decoupling exhibit a broad signal in the range −525 to −660 ppm with the maximum centering at around −600 ppm. This value matches well with the isotropic resonance observed for pure SnO_2.[24,25] Furthermore, in many ternary tin oxides, the octahedral Sn resonates in the chemical shift range of −450 to −700 ppm. In view of these facts, it can be concluded that the Sn is present in an octahedral environment in both of these samples. However, the broadening of the signal could be due to either (i) lowering of local symmetry of the Sn nuclei or (ii) magnetic interaction with neighboring proton (H) nuclei, since the compounds are composed of Mg−Al−Sn−(OH)−CO_3 (for Sn 3-LDH) and Mg−Sn−(OH) (for Sn 10-LDH). To identify the cause for broadening of the signals, proton-decoupled spectra were recorded for both samples. It can be seen that there is not much change in the spectral pattern in the case of Sn 3-LDH upon proton decoupling, implying that the broadening is due to the lowering of local symmetry around Sn nuclei. On the contrary, the broadening of the signal is reduced dramatically and

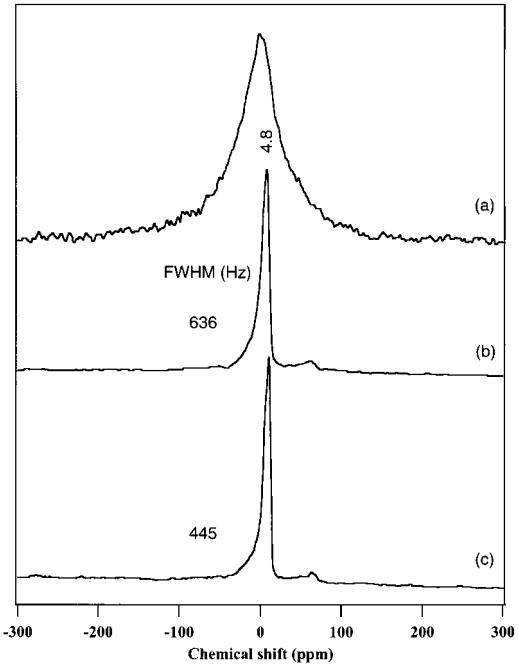

Figure 5. ^{27}Al MAS NMR spectra of (a) Sn 3-LDH (without proton decoupling), Sn 3-LDH (with proton decoupling), and (c) Sn 0-LDH (with proton decoupling).

developed a sharp resonance at −581 ppm in the case of Sn 10-LDH, demonstrating that the Sn nuclei in this compound have a strong magnetic interaction with neighboring H nuclei. Taking into account the difference in chemical composition between Sn 3-LDH and that of Sn 10-LDH, it is reasonable to assume that the observed broad signal in Sn 3-LDH could be due to the possible magnetic interaction with neighboring Al nuclei in the brucite-like layer. Such an interaction is not possible in Sn 10-LDH. It is therefore concluded that the observed broad signal in Sn 3-LDH is due to the presence of Sn in a distorted octahedral environment as a consequence of isomorphous substitution in the brucite-like lattice. In contrast, Sn exists in a regular octahedral environment in Sn 10-LDH, which possesses the $MgSn(OH)_6$ as a major phase rather than a LDH phase.

^{27}Al MAS NMR has been widely employed to characterize the nature of coordination of Al present in MgAl-LDH, ZnAl-LDH, and their calcined products.[26−28] Both MgAl-LDH and ZnAl-LDH showed a single resonance around 10 ppm for Al existing in an octahedral coordination [Al(oh)]. Upon calcination, these materials develop an additional resonance around 60 ppm for tetrahedral Al [Al(td)]. The ^{27}Al MAS NMR spectra of Sn 0-LDH and Sn 3-LDH in the present study are presented in Figure 5. They show a sharp and single resonance around 5−7 ppm together with a small resonance around 62 ppm (spinning sidebands are expected around 60−70 ppm), indicating that most of the Al are present in the octahedral coordination. Although there is no much difference in chemical shift values upon Sn incorporation, an increase in the octa-

(24) Clayden, N. J.; Dobson, C, M.; Fern, A. *J. Chem. Soc., Dalton Trans.* **1989**, 843.
(25) Mal, N. K.; Veda Ramaswamy, Ganapathy, S.; Ramaswamy, A. V. *Appl. Catal. A: General* **1995**, *125*, 233.
(26) Mackenzie, K. J. D.; Meinhold, R. H.; Sherriff, B. L.; Xu, Z. *J. Mater. Chem*. **1993**, *3*, 1263.
(27) Velu, S.; Ramkumar, V.; Narayanan, A.; Swamy, C. S. *J. Mater. Sci*. **1997**, *32*, 957.
(28) Weir, M. R.; Kydd, R. A. *Inorg. Chem*. **1998**, *37*, 5619.

Table 2. Textural Properties of MgAlSn-LDHs

sample	N_2 adsorption measurements	
	BET SA[a] ($m^2\ g^{-1}$)	SPPV[a] ($cm^3\ g^{-1}$)
Sn 0-LDH	92	0.570
Sn 1-LDH	86	0.445
Sn 2-LDH	63	0.412
Sn 3-LDH	44	0.279
Sn 5-LDH	65	0.337
Sn 10-LDH	46	0.247
Al 7-LDH	88	

[a] BET surface area and specific pore volume (SPPV) of samples degassed at 30 °C/10 h.

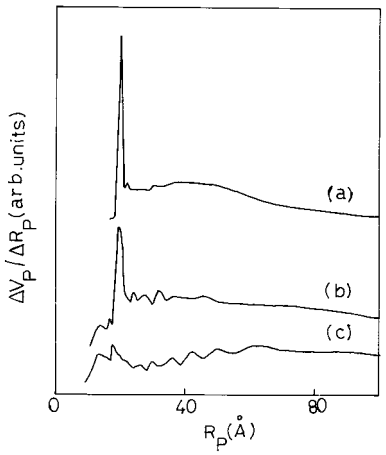

Figure 6. Pore size distribution curves of (a) Sn 0-LDH, (b) Sn 3-LDH, and (c) Sn 10-LDH.

hedral line width is envisaged. For example, the fwhm value of Sn 0-LDH, without Sn, is 445 Hz, while the same for Sn 3-LDH is 636 Hz. Such an increase in line width can be attributed to the distortions in the local environment of Al induced by the incorporation of Sn in the MgAl-LDH lattice. It is also interesting to note that, unlike ^{119}Sn NMR, the ^{27}Al NMR spectra of Sn 3-LDH shows a dramatic change in line width of NMR signal upon proton decoupling. This indicates that the ^{27}Al nuclei experience relatively stronger magnetic interaction with neighboring protons existing in the brucite-like layer as compared to that of ^{119}Sn nuclei.

The surface textural properties of Sn-containing LDHs are assessed by the N_2 adsorption−desorption measurements at liquid N_2 temperature. These compounds showed isotherms corresponding to type IV in the IUPAC classification,[29] indicating that the materials are mesoporous in nature.[30] The BET surface area and specific pore volume (SPPV) determined from these isotherms are gathered in Table 2, while their pore size distribution curves of representative sample are presented in Figure 6. It can be seen that both Sn 0-LDH and Sn 3-LDH exhibit an "unimodel" distribution of pores with a sharp peak centered around 20 Å. On the other hand, Sn 10-LDH, which showed the $MgSn(OH)_6$ as the major phase in PXRD, exhibits a weak rise and a wide range of pore radius (15−60 Å). It can be noticed from Table 2 that the BET surface area and SPPV decrease with an increase in Sn content in the sample.

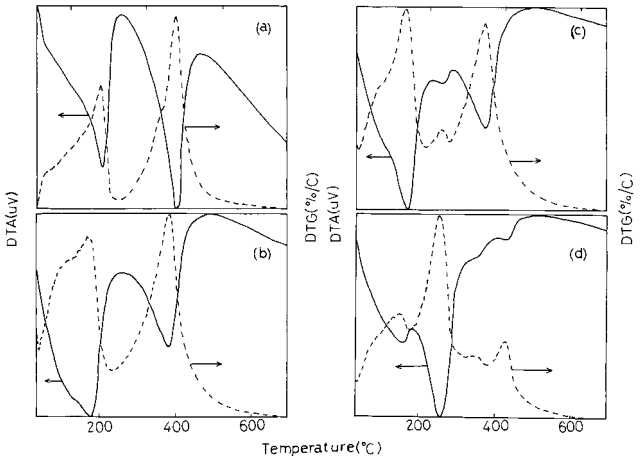

Figure 7. DTG (- - -) and DTA (—) traces of (a) Sn 0-LDH, (b) Sn 3-LDH, (c) Sn 5-LDH, and (d) Sn 10-LDH.

These results reveal that the surface textural properties are affected by the Sn incorporation in the MgAl-LDH framework.

The thermal stability of these Sn-containing LDHs was examined by simultaneous TG/DTA experiments. Figure 7 depicts the differential curve of the TG (DTG) and the DTA curve of a few representative samples. It can be seen that DTA curves are exactly the mirror image of DTG curves, demonstrating the coincidence of the weight loss process in TG with that of enthalpy change occurring in DTA. The DTG/DTA of Sn 0-LDH to Sn 3-LDH shows two strong endothermic transitions characteristic of LDHs. The first endothermic transition observed in the temperature range 160−200 °C is attributed to the dehydration process, while the second endothermic peak within 360−410 °C is ascribed to the dehydroxylation and decarbonation processes. In TG they are related to the loss of interlayer water (T_1) and the removal of structural water and CO_2 from the interlayer (T_2), respectively.[19,31] However, an additional endothermic peak is observed around 250 °C in Sn 4-LDH, in which a mixture of HT and MHS phases is detected by PXRD. The intensity of this peak increases with further increase in Sn content in the sample, and it is the strongest endothermic peak registered in the case of Sn 10-LDH. This additional endothermic transition can be attributed to the dehydroxylation of $MgSn(OH)_6$ (based on our PXRD results). The absence of such an endothermic peak in the samples Sn 0-LDH through Sn 3-LDH implies that LDH is the only phase formed; even a trace of X-ray amorphous Sn-containing phase has not been formed in these compounds. On the basis of our PXRD and TG/DTA results, it can be concluded that, under the preparation conditions employed in the present study, up to at least 30% of the Al^{3+} in the brucite-like layer is isomorphously substituted by Sn^{4+} ion to form a single phase corresponding to Mg−Al−Sn ternary LDH. Further increase in Sn content results in the coformation of the MHS phase together with the LDH phase. From chemical analysis and percent weight loss measured in TG, the chemical formulas of the Sn-incorporated LDHs are calculated and are included in Table 1 itself together with other structural properties.

(29) Sing, K. S. W.; Everett, D. H.; Haul, R. A. W.; Moscou, L.; Pierotti, R. A.; Rouquerol, J.; Sieminiewska, T. *Pure Appl. Chem*. **1985**, *57*, 603.

(30) Leofanti, G.; Padovan, M.; Tozzola, G.; Venturelli, B. *Catal. Today* **1998**, *41*, 207.

(31) Cavani, F.; Trifiro, F.; Vaccari, A. *Catal. Today* **1991**, *11*, 173.

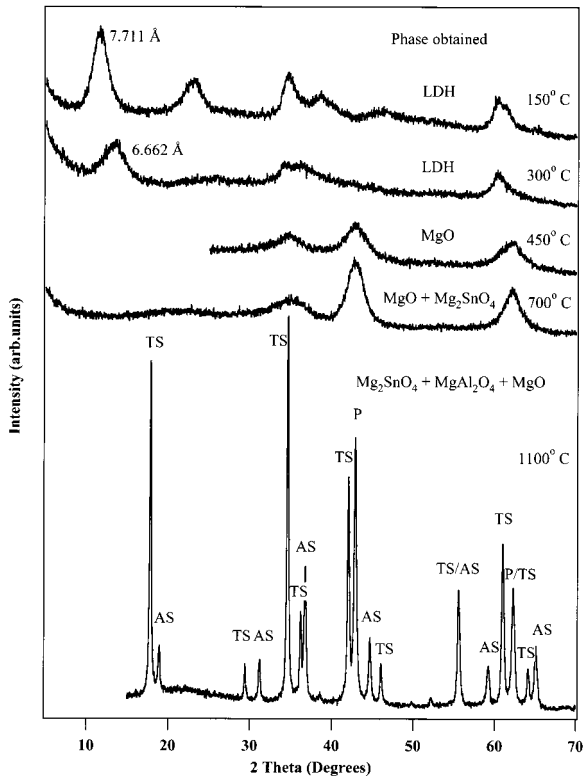

Figure 8. PXRD patterns of Sn 3-LDH calcined at various temperatures: LDH = layered double hydroxide; (P) = MgO; (AS) = $MgAl_2O_4$; (TS) = Mg_2SnO_4.

Thermal Evolution. Thermal calcination of LDHs often produces very reactive mixed oxides depending upon the calcination temperature.[1,31,32] The determination of crystalline phases formed during calcination at various temperatures is useful to assess the thermal stability of the materials. For this purpose the sample Sn 3-LDH was subjected to calcination at various temperatures for 5 h in air; their PXRD patterns are shown in Figure 8. The removal of physisorbed water at 150 °C does not modify the layer structure. Only a small decrease in the basal spacing [*d*(003)] from 7.84 to 7.711 Å is noticed, indicating that a minor amount of interlayer water is lost at this temperature. At a calcination temperature of 300 °C, the dehydration process (as evidenced from TG/DTA) induces a decrease in basal spacing of about 1 Å (a shift from 7.711 to 6.662 Å). At the same time the (10*l*) reflections at higher 2θ angle are also shifted and become broader due to some disorder in the structure, but still retaining the characteristics of layer structure. However, for the samples calcined at 450 °C (herein after referred to as LDHcal), the absence of diffraction peaks corresponding to LDH phase revealed that the layer structure is completely destroyed due to the removal of structural water and CO_2 from the interlayer (the T_2 process in TG/DTA). This also caused an increase in BET surface area from about 40 to 200 $m^2\ g^{-1}$ at 450 °C (see Figure 9) because of the formation of a cratered surface perpendicular to the basal planes.[33] For this calcination temperature two broad diffraction lines are observed, which corresponded to the *d*(200) and *d*(220) reflections of a mixed oxide

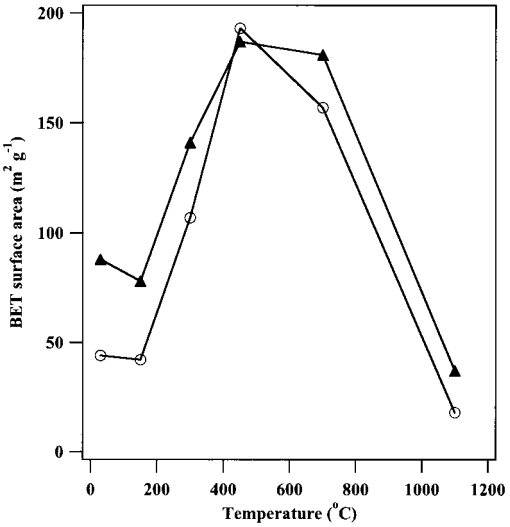

Figure 9. Surface area evolution with temperature for (○) Sn 3-LDH and (▲) Al 7-LDH.

phase with MgO-like structure. It must be stressed that, in addition to the MgO-like phase, amorphous phases can be present and even preponderant. The lattice constant of the MgO-like phase formed at this temperature is 4.223 Å, which is higher than that of the pure MgO (4.211 Å), indicating that a small amount of Sn^{4+} is dissolved in the lattice to form a solid solution. The sharpness of the peaks increases with increase in the calcination temperature to 700 °C, in line with the results of progressive increase of the crystallinity due to sintering of the material as evidenced from a drop in the BET surface area (Figure 9). The observed lattice parameter of the MgO-like phase at this temperature is 4.220 Å. So, for the samples calcined between 450 and 700 °C only the MgO-like mixed oxide phase is observed. However, earlier reports[34] on MgAl-LDH and NiMgAl-LDH by neutron diffraction studies have attributed the formation of defective spinel like phase with cation vacancies in the octahedral sites around 700 °C. The formation of discrete Al/Sn-containing phases are not detected by PXRD of our samples; possibly, they are present in the microdomains of the crystalline phase. For the samples calcined at 1100 °C, the spectrum shows a mixture of well-crystallized phases similar to MgO, $MgAl_2O_4$ spinel (AS), and Mg_2SnO_4 (TS). It should be mentioned that the preferred structure of $MgAl_2O_4$ is a normal spinel,[35] wherein the Mg^{2+} and Al^{3+} occupy the tetrahedral and octahedral sites, respectively. On the other hand, the Mg_2SnO_4 is an inverse spinel; the tetrahedral sites are occupied by only one-half of the Mg^{2+} ions, while the rest of the Mg^{2+} ions, together with all the Sn^{4+} ions, are randomly distributed over octahedral sites. The lattice parameters of all these three phases were calculated from their prominent peaks in PXRD, and the values are compared with those given in the literature (Table 3). It is interesting to note that the calculated lattice constant of the $MgAl_2O_4$ phase is 8.093 Å, larger than the value given in the literature (8.083 Å). In contrast, the observed lattice constant of Mg_2SnO_4 (8.584 Å) is less than that of the literature

(32) Kannan, S. *Appl. Clay Sci.* **1998**, *13*, 347.
(33) Belloto, M.; Rebours, B.; Clause, O.; Lynch, J.; Bazin, D.; Elkaim, E. *J. Phys. Chem.* **1996**, *100*, 8535.
(34) Gazzano, M.; Kagunya, W.; Matteuzzi, D.; Vaccari, A. *J. Phys. Chem. B* **1997**, *101*, 4514.
(35) Greenwood, N. N. *Ionic Crystals Lattice defects and Nonstoichiometry*; Butterworths: London, 1968.

Table 3. Observed Lattice Parameters of Phases Formed in Sn 3-LDH Calcined at 1100 °C/5 h

phase obtained	obsd *a* value (Å)	lit. *a* value (Å)	Δ*a* (Å)
MgO	4.214	4.211	+0.003
$MgAl_2O_4$	8.093	8.083	+0.01
Mg_2SnO_4	8.584	8.638	−0.054

value (8.638 Å). However, in the case of MgO-like phase, the lattice constant is more or less similar to that of a pure MgO, demonstrating that the Sn which earlier dissolved in the MgO lattice up to around 700 °C is now got migrated to form a separate Mg_2SnO_4 spinel phase. The higher "*a*" parameter observed for $MgAl_2O_4$ spinel suggests that a small amount of Al^{3+} is isomorphously substituted by Sn^{4+} in $MgAl_2O_4$ spinel, thereby increasing the lattice constant, as the ionic radius of Sn^{4+} is larger than that of Al^{3+}. In a similar way, Al^{3+} might substitute a small amount of Sn^{4+} in Mg_2SnO_4 spinel. If we consider that all the Sn atoms in these spinel structures are present in the +4 oxidation state, then the approximate chemical compositions of the spinels, $MgAl_2O_4$ and Mg_2SnO_4, can be derived to be $MgAl_{(2-4x)}Sn_{3x}O_4$ and $Mg_2Sn_{(1-3x)}Al_{4x}O_4$, respectively. These chemical compositions would satisfy the observed difference in the lattice parameters. It is clear from the Table 3 that a large difference (0.054 Å) in lattice parameter is noticed in the case of Mg_2SnO_4 compared to any other phase. Hence, a relatively higher amount of Al might be dissolved in the Mg_2SnO_4 phase compared to the amount of Sn dissolved in the $MgAl_2O_4$ phase. It is also interesting to note that the peak intensity of the Mg_2SnO_4 (TS) phase is relatively higher in comparison with that of $MgAl_2O_4$ (AS) phase, despite a low Sn content in the sample. This indicates that the formation of Mg_2SnO_4 spinel is more preferred compared to that of $MgAl_2O_4$ spinel in these materials.

The change in chemical environments around Sn and Al during calcination has been investigated using ^{119}Sn and ^{27}Al MAS NMR. Because of the complication in obtaining the ^{119}Sn MAS NMR spectra of calcined samples under our experimental conditions, we have recorded the ^{119}Sn NMR only for Sn 3-LDH calcined at 1100 °C for 5 h. On the other hand, the ^{27}Al MAS NMR spectra were recorded for a few samples calcined at both 450 and 1100 °C. Figure 10 depicts the ^{119}Sn MAS NMR spectra of Sn 3-LDH calcined at 1100 °C for 5 h. It shows the isotropic resonance around −471 ppm along with sidebands. It should be remembered that the PXRD of the sample showed a mixture of well-crystallized phases similar to Mg_2SnO_4, $MgAl_2O_4$ spinels, and MgO. Hence, it is reasonable to assign the observed NMR spectral pattern to the Mg_2SnO_4 spinel phase. In an earlier study,[24] the ^{119}Sn NMR of pure Mg_2SnO_4 exhibited an isotropic resonance at −483.5 ppm together with spinning sidebands. The observed results have been attributed to Sn existing in an octahedral coordination, but the SnO_6 octahedra are distorted in both bond lengths and bong angles. Our results are in consistent with this literature report, exhibiting a similar NMR pattern corresponding to the Mg_2SnO_4 spinel. However, the observed chemical shift value is lower by about 12 ppm.

Figure 11 shows the ^{27}Al MAS NMR spectra of samples calcined at 450 and 1100 °C. The spectrum shows evidence for the presence of both Al(td) ($\delta \approx 67$ ppm) and Al(oh) ($\delta \approx 10$ ppm). The appearance of Al(td) is more pronounced in these calcined samples compared to the uncalcined counterparts. It is believed that as the interlayer carbonate anions are evolved as CO_2 during calcination, the Al^{3+} cations migrate into the gallery space and adopt a tetrahedral coordination.[28,33] It should be recalled that MgO is the only phase detected from PXRD (see Figures 8 and 12). No separate crystalline phase exists that could account for the observed Al(td). However, an amorphous phase similar to γ-Al_2O_3 could possibly occur in the microdomains of the MgO phase,[36,37] leading to the observed broadening

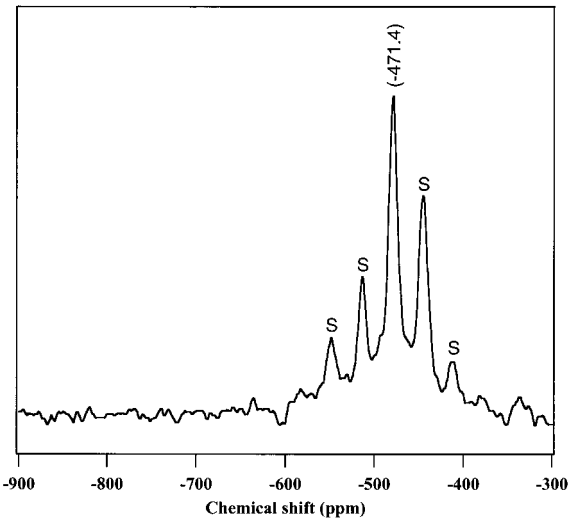

Figure 10. ^{119}Sn MAS NMR of Sn 3-LDH calcined at 1100 °C for 5 h. (S) = spinning sidebands.

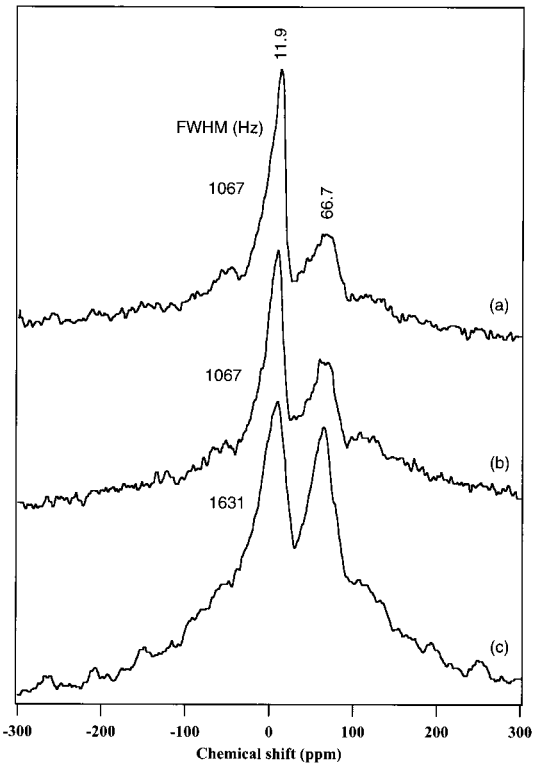

Figure 11. ^{27}Al MAS NMR of (a) Sn 0-LDHcal, (b) Sn 3-LDHcal, and (c) Sn 3-LDH calcined at 1100 °C for 5 h.

(36) Mckenzie, A. L.; Fishel, C. T.; Davis, R. J. *J. Catal.* **1992**, *138*, 547.

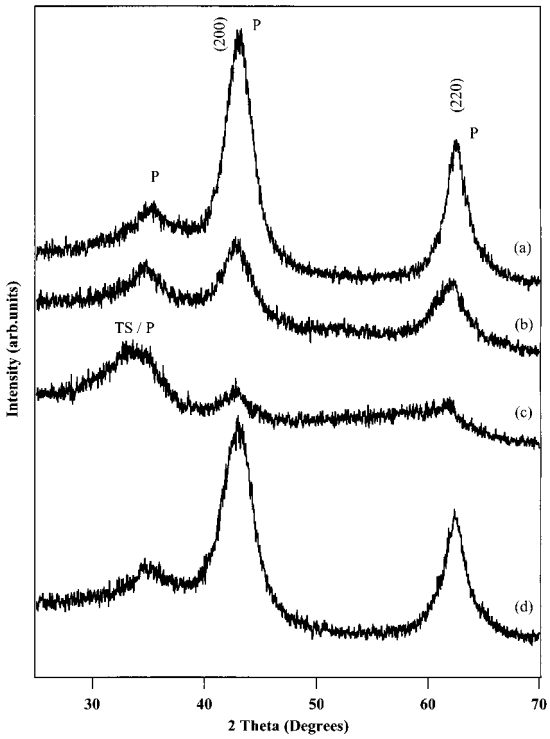

Figure 12. PXRD patterns of (a) Sn 0-LDHcal, (b) Sn 3-LDHcal, (c) Sn 10-LDHcal, and (d) Al 7-LDHcal; (P) = MgO; (TS) = Mg_2SnO_4.

of those reflections in PXRD and also broadening of the Al(td) and Al(oh) resonance peaks. Although there is not much difference in the NMR pattern between Sn 0-LDHcal and Sn 3-LDHcal, it is interesting to compare the NMR spectra of these compounds with those of the uncalcined counterparts (compare Figures 6 and 11). A downfield shift for both Al(td) and Al(oh) resonance peaks and a 2−3-fold increase in line width of Al(oh) are noticed upon calcination. These results suggest a deformation in coordination sphere around Al nuclei, possibly due to the formation of MgO solid solution, in which Al^{3+} ions occupy the sites of the MgO lattice at 450 °C as evidenced by PXRD. Calcination at 1100 °C results in a further increase in intensity of the Al(td) resonance. This is in contrast to an earlier report by Mackenzie et al.,[26] who observed a decrease in Al(td) resonance intensity because of the formation of $MgAl_2O_4$ spinel at this temperature, since in a normal spinel the Al and Mg atoms occupy the octahedral and tedrahedral sites, respectively.[35] However, it is known that a part of Al also occupies tetrahedral sites, leading to disorder in cation distribution. For $MgAl_2O_4$ spinel the cation distribution can be expressed by the formula $[Mg_{(1-x)}Al_x]_{td}$-$[Al_{(2-x)}Mg_x]_{oh}O_4$, where "*x*" is referred to as the "inversion" parameter and can be determined from the ^{27}Al MAS NMR.[38] It should be remembered that the PXRD of the sample calcined at 1100 °C showed a mixture of phases similar to MgO, $MgAl_2O_4$, and Mg_2SnO_4. The observed Al(td) resonance is thus assigned to the $MgAl_2O_4$ spinel with large disorder in cation distribution. Hence, it is reasonable to conclude that the increase in intensity of Al(td) resonance in the present study is because of the increase in the "inversion parameter, *x*". Unfortunately, since the spinning sidebands (around 60−70 ppm) are expected to overlap with that of the Al(td) resonance, under our experimental conditions, it was not possible to calculate the Al(td)/Al(oh) ratio from NMR peaks. The formation of the $MgAl_2O_4$ phase influences a shift of both Al(td) and Al(oh) resonance frequencies toward lower δ value. Similar results were also observed upon incorporation of Zr^{4+} in the MgAl-LDH framework.[13]

On the basis of the PXRD, TG/DTA, ^{119}Sn, and ^{27}Al MAS NMR results, the following reaction scheme can be proposed for the decomposition of Sn 3-LDH at different calcination temperatures:

$$Mg_6Al_{1.40}Sn_{0.58}(OH)_{16}(CO_3)_{1.26}\ 5.9.H_2O$$
$$\approx 300^o\ C \downarrow -\ 5.9\ H_2O$$
$$Mg_6Al_{1.40}Sn_{0.58}(OH)_{16}(CO_3)_{1.26}$$
$$\approx 450^o\ C \downarrow -H_2O/\ CO_2$$
$$MgO\ \text{(solid solution)} + (XAP)$$
$$\approx 700^o\ C \downarrow$$
$$MgO\ \text{(solid solution)} + (XAP)$$
$$\approx 1100^o\ C \downarrow$$
$$MgO + Mg_2Sn_{(1-3x)}Al_{4x}O_4\ \text{spinel} + MgAl_{2-4x}Sn_{3x}O_4\ \text{spinel}$$

where (XAP) represents the X-ray amorphous phase.

LDHs have been employed as catalysts either as such or after a controlled thermal treatment, generally around 450 °C.[1,5,32] At this temperature LDHs lose their layer structure and form highly active mixed oxides with high thermal stability, high surface area, and good metal dispersion which are very important for their catalytic applications. For example, the Al-stabilized MgO obtained by the thermal decomposition of MgAl-LDH around 450 °C has been proposed to be a novel support for Pt or Pd, and the resulting catalyst was found to be active for hydrocarbon reforming reactions.[39] Hence, we payed more insight into the effect of Al/Sn ratio on the structural and surface textural properties of these calcined products. Figure 12 depicts the PXRD patterns of some of the Sn-containing LDHs calcined at 450 °C for 5 h. It can be seen that in all cases the layer structure is completely collapsed and formed a poorly crystallized cubic phase similar to that of MgO. The crystallinity of the resulting cubic phase decreases with increasing Sn content. In the case of Sn 10-LDH, without Al, in addition to the MgO-like phase, a poorly crystallized phase similar to the Mg_2SnO_4 "inverse spinel" is noticed.

It has been known in the literature[21,33,34] that in the case of MgAl systems thermal decomposition around 450 °C yields a poorly crystallized MgO phase whose lattice constant "*a*" is less than that of pure MgO. The decrease in lattice constant has been attributed to the dissolution of a small amount of Al^{3+} in the MgO lattice

(37) Rey, F.; Fornes, V.; Rojo, J. M. *J. Chem. Soc., Faraday Trans.* **1992**, *88*, 2233.
(38) Millard, R. L.; Peterson, R. C.; Hunter, B. K. *Am. Mineral.* **1992**, *77*, 44.
(39) Davis, R. J.; Derouane, E. G. *Nature* **1991**, *349*, 313.

Table 4. Structural and Textural Properties of MgAlSn-LDHcal (LDHs Calcined at 450 °C/5 h)

sample	lattice parameter of MgO-like solid solution[a] (Å)	fwhm (2θ) (200) plane	fwhm (2θ) (220) plane	N_2 adsorption measurements BET SA[b] ($m^2\ g^{-1}$)	SPPV[b] ($cm^3\ g^{-1}$)
Sn 0-LDHcal	4.170	2.254	1.831	234	1.076
Sn 1-LDHcal	4.179	2.264	1.887	218	0.857
Sn 2-LDHcal	4.213	2.642	2.264	202	0.779
Sn 3-LDHcal	4.223	2.817	2.817	193	0.627
Sn 5-LDHcal	4.219	3.019	2.830	165	0.626
Sn 10-LDHcal				150	0.452
Al 7-LDHcal	4.186	2.817	2.083	187	0.972

[a] Calculated from *d*(200) and *d*(220) planes. [b] BET surface area and specific pore volume (SPPV) of samples degassed at 400 °C/5 h.

to form solid solutions. The chemical composition of the resulting solid solution was given by the formula $Mg_{(1-x)/(2+x)}Al_{2x/(2+x)}[\ ]_{x/(2+x)}O$, where [ ] is a cation vacancy created due to the dissolution of a part of Al^{3+} in the MgO lattice.[40] In the present study the *a* parameter of Sn 0-LDH is 4.170 Å, which is less than that of the pure MgO (4.211 Å) and is in accordance with the earlier reports, indicating that a small amount of Al^{3+} is dissolved in the MgO lattice. As the Sn content in the LDH increases, the *a* parameter of the resulting cubic phase also increases and attains a value similar to that of MgO (see Table 4). Since the ionic radius of Sn^{4+} (0.69 Å) is nearly the same as that of Mg^{2+} (0.72 Å),[18] the *a* parameter of the cubic phase reaches the *a* value of MgO even at very low Sn^{4+} content in the sample (Sn 2-LDH). From these results it can be concluded that a part of Sn^{4+}, in addition to Al^{3+}, dissolves in the MgO lattice to form Mg−Al−Sn−O and/or Mg−Sn−O solid solution similar to the composition described above. Interestingly, these solid solutions upon rehydration in water revert back to form the original LDH structure. This phenomenon is referred to as "memory effect" and is a characteristic of HT-like materials.[31] However, it is yet unclear whether Sn is incorporated during reconstruction. Detailed study along this line is underway, and the results will be reported at a later date.

The N_2 adsorption−desorption experiments on calcined samples showed isotherms similar to those observed for as-synthesized counterparts. The pore size distribution curves of some of these calcined samples are presented in Figure 13. The observed results are in contrast to those noticed in their as-synthesized counterparts. Sn 0-LDH exhibits a very broad distribution of pores in the range 20−80 Å with a very small rise, while both Sn 3-LDHcal and Sn 10-LDHcal exhibits a sharp peak around 20 Å. The BET surface area and SPPV of these calcined LDHs are summarized in Table 4. Similar to those observed in the as-synthesized samples, both BET surface area and SPPV were found to decrease with increase in Sn content. However, compared to the as-synthesized samples, the calcined

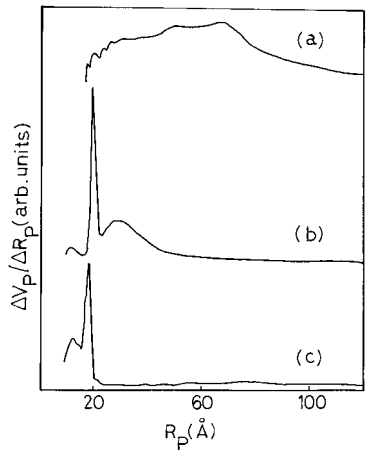

Figure 13. Pore size distribution curves of (a) Sn 0-LDHcal, (b) Sn 3-LDHcal, and (c) Sn 10-LDHcal.

samples exhibit higher BET surface area and SPPV because of the evolution of CO_2 and H_2O gases during the thermal decomposition of LDHs at 450 °C.

In brief, thermal calcination of MgAlSn-LDHs up to 700 °C offers MgO-like solid solution in which a part of Sn^{4+}/Al^{3+} is dissolved. At 1100 °C, nonstoichiometric spinel phases similar to $MgAl_2O_4$ and Mg_2SnO_4 are obtained along with the MgO-like phase. The structural and surface textural properties depend strongly on the Sn content in the sample.

Conclusions

A new series of Sn-incorporated LDHs have been synthesized by coprecipitation. The structural and surface textural properties of these Sn-containing LDHs depend strongly on the Sn content in the sample. A single phase corresponding to LDH is obtained when a part of Al^{3+} (nearly 30%) in the Mg−Al layer is isomorphosly substituted by Sn^{4+}. Higher concentration of Sn results in the coformation of the $MgSn(OH)_6$ phase along with the LDH phase. The Sn atoms in the LDH framework are existing in a distorted octahedral environment.

Thermal calcination of these Sn-containing LDHs at 450 °C gives rise to a MgO-like phase, in which a part of Al^{3+}/Sn^{4+} is dissolved to form a solid solution. This also leads to deformation in the coordination spheres of Al and Sn nuclei. The surface properties such as BET surface area and pore volume increase upon calcination because of the evolution of CO_2 and H_2O gases by the decomposition of the layer structure. The incorporation of Sn results in a decrease in surface area and pore volume of both as-synthesized and in calcined samples. Calcination of MgAlSn-LDHs at 1100 °C leads to the formation of nonstoichiometric spinels such as $MgAl_2O_4$ and Mg_2SnO_4 "inverse spinel" along with the MgO phase.

Acknowledgment. S.V. is grateful to the Science and Technology Agency of Japan for the award of an STA fellowship.

CM990067P

(40) Constantino, V. R. L.; Pinnavaia, T. J. *Catal. Lett.* **1994**, *23*, 361.